Intensity Considerations in Liquid Core Optical Fiber Raman Spectroscopy

ROBERT ALTKORN,* MICHELLE DUVAL MALINSKY, RICHARD P. VAN DUYNE,* and ILIA KOEV

Department of Physics and Astronomy, Northwestern University, 1801 Maple Ave., Evanston, Illinois 60201 (R.A.); Department of Chemistry, Northwestern University, 2145 Sheridan Road, Evanston, Illinois 60208 (M.D.M., R.P.V.); and Biogeneral Inc., 9925 Mesa Rim Road, San Diego, California 92121 (I.K.)

This paper develops expressions for the Raman power emitted by liquid core optical fiber (LCOF) sample cells in six simple excitation/collection geometries and the fraction of that power that can be utilized in a conventional Raman spectrometer. From these expressions a "figure of merit" is developed that can be used to predict the relative intensity enhancement provided by LCOFs having different inside diameters and loss characteristics. For the apparatus used here, we show theoretically and experimentally that the figure of merit takes the simple form $(\alpha d)^{-1}$ where α and d are, respectively, the loss coefficient and inside diameter of the LCOF. Given the varying optical quality of Teflon®-AF LCOFs currently in use, the analysis presented here should be useful in optimizing the performance of LCOF accessories in Raman and related spectroscopic applications.

Index Headings: **Liquid core optical fibers; LCOFs; Raman spectroscopy.**

INTRODUCTION

Capillary cells designed to promote total internal reflection within sampled liquids, often referred to as liquid core optical fibers (LCOFs), liquid core waveguides, or waveguide capillary cells, have been used in Raman spectroscopy for nearly 70 years.[1] When compared to conventional sample cells, these waveguide cells have been shown to provide much higher Raman signal intensities and signal-to-noise ratios while simultaneously reducing sample volume requirements. The popularity of these cells has varied, probably peaking between the mid-1950s and the early 1970s with their use as standard accessories for the Cary 81 lamp- and laser-excited Raman spectrophotometers.[2–5] However, the most significant technical advance in waveguide capillary sampling came at the end of this period when Walrafen and Stone[6,7] used fused-silica liquid core optical fibers up to 25 m in length to acquire Raman spectra of two high-refractive-index liquids: benzene ($n_D^{20} = 1.50$) and tetrachloroethylene ($n_D^{20} = 1.51$). The cells used by Walrafen and Stone produced intensity enhancements of as much as 3000 relative to conventional sampling arrangements and have yet to be surpassed in performance. Unfortunately, these cells are suitable only for liquids having refractive indices higher than that of fused silica ($n_D \cong 1.46$), and therefore have only been used sporadically. The authors recognized the limitations of their devices and recommended replacing fused silica with a lower-refractive-index material, such as Teflon®. However, at the time of their work, low-refractive-index capillaries of suitable optical quality were unavailable.[8]

Within the last four years a group of LCOFs made from the low-refractive-index amorphous fluoropolymer Teflon®-AF 2400 ($n_D = 1.29$) have been used in Raman applications.[9–16] At their current state of development, these Teflon® LCOFs exhibit substantially higher losses than their earlier fused-silica counterparts. Despite this disadvantage, Teflon®-AF LCOFs provide much greater materials compatibility and yield up to 500-fold Raman intensity enhancements and commensurate improvements in signal-to-noise ratio when used with various low-refractive-index liquids, including aqueous solutions. Thus, Teflon®-AF LCOFs offer outstanding promise in numerous applications of Raman spectroscopy. Specifically, the areas most likely to benefit from the use of the LCOFs include the following: (1) biological applications, where low solubilities and denaturing at high laser power often mandate the use of nonstandard sampling techniques; (2) environmental monitoring, which necessitates the ability to detect low-level analyte concentrations in aqueous solutions; (3) low-cost systems, where the intensity enhancement provided by LCOFs might enable the use of less expensive lasers and/or detectors; and (4) high-performance liquid chromatography (HPLC), where convenient geometry, small volume, and improved signal intensity and signal-to-noise ratio combine to make Raman detection attractive.

In spite of the long history and current resurgence of interest in LCOFs, surprisingly little effort has been directed towards analyzing the intensity advantages that these devices can provide. Indeed, the Raman enhancement factors reported for LCOFs have varied over a wide range (one to three orders of magnitude) for reasons that do not seem entirely clear.[6,13] The goal of this paper is to

Received 9 October 2000; accepted 21 December 2000.
* Authors to whom correspondence should be sent.

0003-7028/01/5504-0373$2.00/0

develop a method for estimating the utilizable Raman power that LCOFs can deliver to spectrometers or spectrographs. Although some spectrometers have been developed specifically for use with waveguide cells,[2,3,17–20] it will be assumed here that it will generally be necessary to interface LCOFs to existing instruments for which factors such as slit size and f/# have been predetermined by other considerations. The problem of determining utilizable Raman intensity is divided into two parts. The first addresses the total Raman power emitted by the LCOF, which is a function of the following parameters: LCOF length, LCOF loss coefficients at the laser and Raman wavelengths, sampling geometry (forward scattering, backward scattering, combined forward and backward scattering, etc.), and input laser power. We will specifically develop expressions for an "effective" LCOF length which is directly proportional to the Raman intensity, for six different simple scattering geometries. The second part of this paper focuses on developing an LCOF "figure of merit" that can be used to compare the relative intensity enhancements that different LCOFs will provide in a given spectroscopic system. Neglecting reflection losses, this quantity is primarily dependent upon intrinsic features of the LCOF—namely, the numerical aperture and inner diameter—and the coupling optics used to match the LCOF to the spectrometer or spectrograph. It will be shown that in many cases spectroscopic instruments are unable to utilize all of the Raman light emitted by an LCOF, even if transfer optics are completely optimized. Additionally, we will demonstrate that the figure of merit is inversely proportional to the product of the LCOF loss coefficient and inner diameter for a conventional scanning double monochromator Raman instrument.

EXPERIMENTAL

The sections of Teflon®-AF 2400 capillary tubing used in this work were manufactured by the drawing technique described previously[9] as well as a new extrusion technique that yields superior quality tubing. The water-clear, highly flexible tubing used in the experiments presented here varied in quality as characterized by the measured loss coefficient, α, which will be discussed later in this report. The overall length and the inner diameter of the LCOFs made from the tubing ranged from 75 to 200 cm and 150 to 533 μm, respectively.

LCOFs were formed by mounting the Teflon®-AF tubing in end cells similar to those used previously.[9,21] The end cells are based on standard 1/16 in. HPLC tees fitted with small adapters having inner diameters slightly larger than the outer diameters of the tubing. These "front end" cells are terminated in 150 μm thick fused-silica windows where the light exits the LCOF to be imaged onto the spectrometer. Unlike the somewhat smaller SMA connector devices used elsewhere, these cells use O-ring seals rather than epoxy, which allows the windows to be removed for cleaning. Laser light was launched into the LCOFs with the use of sections of polyimide-coated silica optical fiber from Polymicro Technologies (FVP series with 0.22 numerical aperture). In all cases, the silica fibers carrying the laser light were inserted directly into the Teflon®-AF tubing. The diameter of the silica fiber varied depending on the inner diameter of the tubing. The Teflon®-AF tubing was filled with methanol using a peristaltic pump fitted with silicone rubber tubing, and flow was maintained throughout all experiments.

Raman spectra of methanol (Aldrich spectrophotometric grade, $n = 1.33$) were acquired in forward scattering geometry with the use of the 514.5 nm line of an argon-ion laser (Spectra-Physics 2060) and a 0.75 m scanning double monochromator (SPEX 1400-2). Spectral resolution of 1 cm^{-1} was achieved by setting both the entrance and exit slits of the monochromator to 40 μm and the internal slit to 80 μm. The LCOF end cell was placed approximately 39 cm from the spectrometer entrance slit. Light emitted from the LCOFs was imaged onto the entrance slit of the spectrometer with the use of an f/1.5 Karl Meyer camera lens centered approximately 7 cm from the end cell, which produced in image magnification of 5.3 at the slit entrance. No attempt was made to eliminate either the laser radiation or the Raman bands generated in the silica optical fiber. In order to determine the maximum Raman intensity and LCOF loss, the silica fiber was moved forward inside the Teflon®-AF tubing in steps of 5 to 10 cm, thereby effectively shortening the length of the LCOF.

RESULTS AND DISCUSSION

Optical Characteristics of the LCOF. In this section, we develop expressions for the Raman radiance, Raman power, and optical conductance of an LCOF for six different sampling geometries. The Raman radiance, L_R (W cm^{-2} sr^{-1}), is a term specifying the Raman power per unit area per solid angle. Intuitively, the Raman power, P_R (W), describes the amount of emitted Raman light that is spread over a surface. It is directly proportional to the intensity measured by the detector (usually given in units of counts or counts s^{-1}). The optical conductance, G (cm^2 sr), characterizes the ability of an optical system to accept light and describes the throughput through an optical train.[22] For the expressions given below, we assume that the LCOF is filled with a solution consisting of a solvent and an analyte; however, only the Raman radiation scattered by the analyte will be considered.

First, we consider a short cylindrical section of an LCOF core uniformly illuminated by a laser. A schematic diagram of a section of LCOF is shown in Fig. 1. Using the derivation developed by Schrader,[23] we define the Raman radiance at each circular face of the cylinder as

$$L_{R,int} = \frac{P_L s}{\pi r^2}\Delta z \qquad (1)$$

The parameters in Eq. 1 are $L_{R,int}$ = Raman radiance *inside* the LCOF core; P_L = laser power; r = LCOF core radius; Δz = illuminated LCOF length ($\ll r$); and s = Raman scattering coefficient (sr^{-1} cm^{-1}), defined as

$$s = \left[\left(\frac{d\sigma}{d\Omega}\right)_k \cdot (\bar{\nu}_{ref} - \bar{\nu}_k)^{-4}\right] \cdot (\bar{\nu}_L - \bar{\nu}_k)^4 \cdot \left[\frac{(n_{co}^2 + 2)^4}{81}\right] \cdot N_A \qquad (2)$$

The variables in Eq. 2 are as follows: $(d\sigma/d\Omega)_k$ = differential scattering cross section (cm^2 sr^{-1}) of the kth vibrational mode of the analyte molecule; ν_{ref} = excitation frequency (cm^{-1}) used to measure $(d\sigma/d\Omega)_k$; ν_k = vibrational

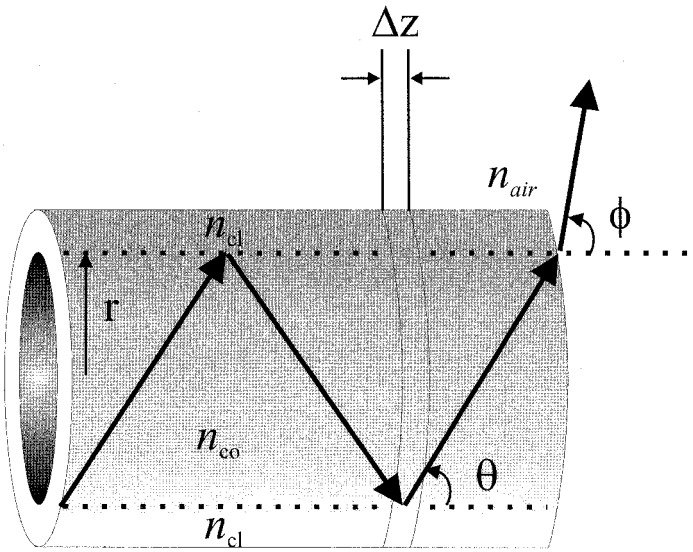

FIG. 1. Schematic diagram of a section of an LCOF waveguide.

frequency (cm^{-1}) of the kth mode; ν_L = frequency of the laser used to excite scattering in the LCOF; n_{co} = refractive index of the LCOF core (assumed for simplicity to be the same at both the laser and Raman wavelengths); and N_A = number density of analyte molecules (cm^{-3}).

The first term in square brackets in Eq. 2 is the "absolute Raman scattering cross section" (cm^6 sr^{-1}) of the kth mode of the analyte molecule. This quantity is approximately wavelength independent in the absence of resonance or preresonance effects and has been tabulated for a number of molecules by Schrötter and Klockner[24] and Schrader[23]. The second term in square brackets is the "internal field factor".[23,25,26]

"Short" LCOFs. Next, we consider a section of LCOF that is long compared to its radius but still is sufficiently short to ensure that attenuation at the laser and Raman wavelengths is negligible. We adopt the meridional ray approximation and assume that there exists a critical angle between the direction of a given light ray and the LCOF axis so that all rays having angles smaller than the critical angle are captured within the LCOF core and all rays at higher angles are lost. In a section of LCOF of physical length z_p, the radiance at each of the circular faces inside the core is given by

$$L_{R,int} = \frac{P_L s}{\pi r^2} z_p \tag{3}$$

for angles smaller than the critical angle and 0 for higher angles. At this point, we make the following assumptions: (1) the Raman radiation passes out of the LCOF and into the air through a nonfocusing window; (2) reflections at the window can be neglected; (3) the radiance of the LCOF end face decreases by a factor of $1/n_{co}^2$ as the captured Raman light expands into a larger solid angle upon exiting the LCOF;[23,26,27] (4) the radiation pattern outside the LCOF can be approximated by a uniformly illuminated cone; and (5) the small angle approximation (sin $\Theta \cong \Theta$) is valid for the cone of emitted light. (This is a good approximation for a Teflon®-AF 2400 LCOF filled with water, where the half-angle subtended by the emitted radiation is approximately 19°.) Under these conditions, the solid angle (sr) subtended by the emitted light is given by

$$\Omega \cong \pi NA^2 = \pi(n_{co}^2 - n_{cl}^2) \tag{4}$$

The variables in Eq. 4 are as follows: Ω = solid angle $= 2\pi(1 - \cos\phi) \cong \pi\phi^2$, where ϕ is the apical half angle of the cone of emitted light; NA = numerical aperture of LCOF $= n_{air}\sin\phi \cong \phi$; n_{co} = refractive index of LCOF core (1.33 for water); and n_{cl} = refractive index of LCOF cladding (1.29 for Teflon®-AF 2400).

(The relationship between NA and core/cladding refractive indices is derived in numerous optical fiber texts.[28]) We now can express the Raman radiance, L_R *outside* each face of a "short" LCOF (in air) as the following:

$$L_R = \frac{P_L s}{\pi n_{co}^2 r^2} z_p \tag{5}$$

The optical conductance, G, can be defined as

$$G = \Omega\pi r^2 = \pi^2 r^2 (n_{co}^2 - n_{cl}^2) \tag{6}$$

The resulting Raman power, P_R, at each circular face is the product of the Raman radiance and optical conductance, which simplifies to the following expression:

$$P_R = L_R G = \frac{P_L s \pi (n_{co}^2 - n_{cl}^2)}{n_{co}^2} z_p \tag{7}$$

From Eq. 7, it is apparent that the Raman power is directly proportional to the length of the LCOF, z_p.

"Long" LCOFs. As the length of the LCOF is increased to the point where attenuation of the laser and/or Raman radiation becomes significant, Eqs. 5 and 7 are no longer valid. However, it is possible to retain the forms of these equations if we take P_L to be the laser power launched into the LCOF and replace the physical LCOF length, z_p, by an "effective" LCOF length, z_e, given by

$$z_c = \int_{z=0}^{z=z_p} T_L(z) \cdot T_R(z)\, dz \tag{8}$$

where $T_L(z)$ and $T_R(z)$ describe the propagation characteristics of the laser and Raman radiation in the LCOF. $T_L(z)$ is the ratio of the laser power at point z in the LCOF to the power launched into the LCOF. Similarly, $T_R(z)$ is the fraction of Raman power captured at point z within the LCOF that is transmitted to the "detector" end of the LCOF. Unlike previous works, which assume single exponential decay, Eq. 8 can accommodate LCOFs in which inhomogeneous,[9] bi-exponential,[29,30] or nonlogarithmic[31] transmission characteristics are observed.

Figure 2 illustrates six simple scattering geometries. We evaluate the effective LCOF lengths as functions of physical LCOF length for each of the experimental configurations shown in Fig. 2. For these derivations, we assume that single exponential decay dominates the transmission properties. (Exponential decay occurs in cases where the loss mechanisms are constant along the length of the LCOF and has been observed in the present work as well as previous work with Teflon®-AF LCOFs.[9,10]) Additionally, we consider instances in which LCOF loss coefficients are both the same and different at the laser and Raman wavelengths. The variation in transmission

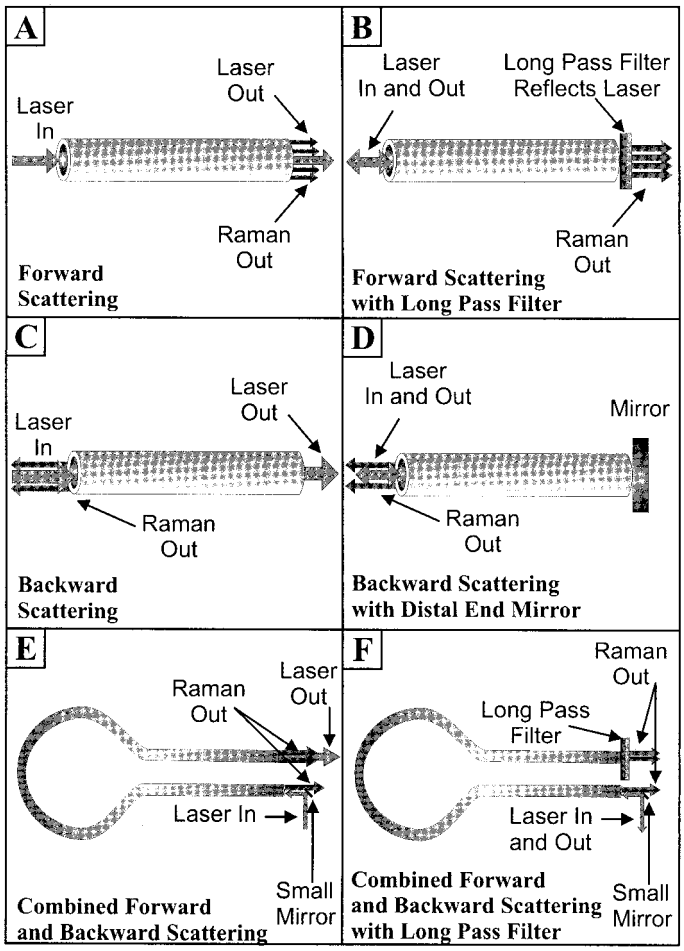

FIG. 2. Schematic diagrams of six excitation/collection geometries considered for the LCOF Raman sample cell. (**A**) Forward scattering; (**B**) forward scattering with a long-pass filter; (**C**) backward scattering; (**D**) backward scattering with a distal end mirror; (**E**) combined forward and backward scattering; (**F**) combined forward and backward scattering with a long-pass filter.

properties between the laser and Raman wavelengths in a given application will depend on the wavelength region and the properties of the core liquid. In many cases, these differences will be negligible. However, over the much wider range of wavelengths commonly used in Raman spectroscopy, the transmission properties will generally vary by well over an order of magnitude. Substantial variation of attenuation with wavelength has been observed in both near-infrared[10,13] and resonance Raman work. Expressions for $T_L(z)$, $T_R(z)$, and z_e are displayed in Table I. In this table, z_p is the physical length of the LCOF Raman cell, α_R is the LCOF's loss coefficient at the Raman frequency, α_L is the cell's loss coefficient at the laser frequency, T is the transmission of the long-pass filter at the Raman wavelength, and R is the reflectivity of the mirror at the Raman and laser wavelengths. Table II presents the maximum effective LCOF length and optimum physical LCOF length for several of these experimental configurations. In deriving the expressions in Tables I and II, we assumed that, in cases where the LCOFs are terminated in mirrors or filters, the intensities of incident and reflected beams add incoherently. In these situations, it is possible for $T_L(z)$ and $T_R(z)$ to exceed unity.

As previously stated (Eqs. 7 and 8), the Raman intensity is proportional to the effective fiber length, z_e. Thus, the relative Raman intensity for each of the various sampling configurations can be compared by examining the z_e. Figure 3 displays a plot of relative Raman intensity as a function of the physical length of the LCOF, z_p, for each of the scattering geometries illustrated in Fig. 2. In this plot, z_p is given in units of attenuation length, which is defined as the physical length of the LCOF at which the laser intensity, I, has decreased to $1/e$ of its original value, I_0. Given the following expression defining the laser intensity at any physical length of LCOF,

$$I = I_0 e^{-\alpha z_p} \tag{9}$$

it is evident that the attenuation length is equal to α^{-1}. For the data shown in Fig. 3, it was assumed that the long-pass filter and mirror behave perfectly where $T = R = 1$. (The long-pass filter transmits 100% of the Raman light and reflects 100% of the laser light. Likewise, the mirror reflects both the Raman and laser light with 100% efficiency.) Additionally, this plot only depicts examples where the attenuation at the Raman and laser wavelengths is the same, $\alpha_R = \alpha_L = \alpha$.

From Fig. 3, it is evident that the Raman intensity as a function of cell length can vary quite significantly depending on the scattering geometry used. To achieve optimal performance, one must consider the specific application goals when an LCOF Raman system is designed. For example, if maximum Raman intensity is the primary experimental goal, clearly the sampling geometry of choice would be the combined forward and backwards scattering that uses a long-pass filter, as shown in Fig. 2F. This geometry provides approximately 60% more Raman intensity at short cell lengths (~ 0.75–1.5 attenuation lengths) when compared to the two next best configurations: (1) combined forward and backward scattering without a filter and (2) backwards scattering with a distal end mirror. However, if the application requires the LCOF to be of significant length, as those used for *in situ* environmental water analysis, then any of the geometries that employ backward scattering would be ideal. Figure 3 demonstrates that the Raman intensity approaches the same value at cell lengths >4 attenuation lengths for any type of backscattering geometry (Fig. 2C–2F). In general, the scattering geometries that use additional optical devices, such as long-pass filters or mirrors, generate approximately 45–50% more Raman light than their counterparts. Because Fig. 3 illustrates only the cases in which the optical device performs perfectly, the quality of the mirror or filter must also be taken into consideration. Furthermore, the designer of the system must account for the complexity of the instrumental apparatus. Although they offer superior overall intensity, geometries such as those shown in Figs. 2E and 2F may be impractical to implement with many Raman systems.

Coupling of the LCOF to the Raman Spectrometer. Perhaps the most fundamental prerequisite to developing an optimized LCOF-based Raman spectroscopy system is determining a "figure of merit" that can be used to predict the relative performance of different liquid core fibers in a particular optical/spectroscopic system. Ideally, this figure of merit should allow a system designer to determine which of several candidate LCOFs would provide the greatest Raman intensity enhancement in a given

TABLE I. Effective fiber lengths for various collection geometries and loss coefficients.

Scattering geometry	$T_L(z)$, $T_R(z)$	Effective fiber length
Forward scattering $\alpha_L = \alpha_R$ Fig. 2A	$T_L(z) = e^{-\alpha z}$ $T_R(z) = e^{-\alpha(z_p - z)}$	$z_e = z_p e^{-\alpha z_p}$
Forward scattering $\alpha_L \neq \alpha_R$ Fig. 2A	$T_L(z) = e^{-\alpha_L z}$ $T_R(z) = e^{-\alpha_R(z_p - z)}$	$z_e = \dfrac{(e^{-\alpha_L z_p} - e^{-\alpha_R z_p})}{\alpha_R - \alpha_L}$
Forward scattering with long-pass filter $\alpha_L = \alpha_R$ Fig. 2B	$T_L(z) = e^{-\alpha z} + Re^{-\alpha(2z_p - z)}$ $T_R(z) = Te^{-\alpha(z_p - z)}$	$z_e = Tz_p e^{-\alpha z_p} + \dfrac{TR}{2\alpha}(e^{-\alpha z_p} - e^{-3\alpha z_p})$
Forward scattering with long-pass filter $\alpha_L \neq \alpha_R$ Fig. 2B	$T_L(z) = e^{-\alpha_L z} + Re^{-\alpha_L(2z_p - z)}$ $T_R(z) = Te^{-\alpha_R(z_p - z)}$	$z_e = T\left[\dfrac{e^{-\alpha_L z_p} - e^{-\alpha_R z_p}}{\alpha_R - \alpha_L} + \dfrac{R(e^{-\alpha_L z_p} - e^{-(2\alpha_L + \alpha_R)z_p})}{\alpha_R + \alpha_L}\right]$
Backward scattering $\alpha_L = \alpha_R$ Fig. 2C	$T_L(z) = e^{-\alpha z}$ $T_R(z) = e^{-\alpha z}$	$z_e = \dfrac{(1 - e^{-2\alpha z_p})}{2\alpha}$
Backward scattering $\alpha_L \neq \alpha_R$ Fig. 2C	$T_L(z) = e^{-\alpha_L z}$ $T_R(z) = e^{-\alpha_R z}$	$z_e = \dfrac{(1 - e^{-(\alpha_L + \alpha_R)z_p})}{\alpha_L + \alpha_R}$
Backward scattering with distal end mirror $\alpha_L = \alpha_R$ Fig. 2D	$T_L(z) = e^{-\alpha z} + Re^{-\alpha(2z_p - z)}$ $T_R(z) = e^{-\alpha z} + Re^{-\alpha(2z_p - z)}$	$z_e = \dfrac{1}{2\alpha}(1 - e^{-2\alpha z_p}) + 2Rz_p e^{-2\alpha z_p} + \dfrac{R^2}{2\alpha}(1 - e^{-2\alpha z_p})e^{-2\alpha z_p}$
Backward scattering with distal end mirror $\alpha_L \neq \alpha_R$ Fig. 2D	$T_L(z) = e^{-\alpha_L z} + Re^{-\alpha_L(2z_p - z)}$ $T_R(z) = e^{-\alpha_R z} + Re^{-\alpha_R(2z_p - z)}$	$z_e = \dfrac{1}{\alpha_R + \alpha_L}(1 - e^{-(\alpha_R + \alpha_L)z_p}) + \dfrac{R}{\alpha_R - \alpha_L}(e^{-2\alpha_L z_p} - e^{-2\alpha_R z_p}) + \dfrac{R^2}{\alpha_R + \alpha_L}(e^{-(\alpha_R + \alpha_L)z_p} - e^{-2(\alpha_R + \alpha_L)z_p})$
Combined forward and backward scattering $\alpha_L = \alpha_R$ Fig. 2E	$T_L = e^{-\alpha z}$ $T_R = e^{-\alpha z} + e^{-\alpha(z_p - z)}$	$z_e = z_p e^{-\alpha z_p} + \dfrac{(1 - e^{-2\alpha z_p})}{2\alpha}$
Combined forward and backward scattering $\alpha_L \neq \alpha_R$ Fig. 2E	$T_L = e^{-\alpha_L z}$ $T_R = e^{-\alpha_R(z_p - z)} + e^{-\alpha_R z}$	$z_e = \dfrac{(e^{-\alpha_L z_p} - e^{-\alpha_R z_p})}{\alpha_R - \alpha_L} + \dfrac{(1 - e^{-(\alpha_L + \alpha_R)z_p})}{\alpha_L + \alpha_R}$
Combined forward and backward scattering with long-pass filter $\alpha_L = \alpha_R$ Fig. 2F	$T_L(z) = e^{-\alpha z} + Re^{-\alpha(2z_p - z)}$ $T_R(z) = Te^{-\alpha(z_p - z)} + e^{-\alpha z} + Re^{-\alpha(2z_p - z)}$	$z_e = \dfrac{1}{2\alpha}(1 - e^{-2\alpha z_p})(1 + R^2 e^{-2\alpha z_p} + TRe^{-\alpha z_p}) + z_p e^{-\alpha z_p}(T + 2Re^{-\alpha z_p})$
Combined forward and backward scattering with long-pass filter $\alpha_L \neq \alpha_R$ Fig. 2F	$T_L(z) = e^{-\alpha_L z} + Re^{-\alpha_L(2z_p - z)}$ $T_R(z) = Te^{-\alpha_R(z_p - z)} + e^{-\alpha_R z} + Re^{-\alpha_R(2z_p - z)}$	$z_e = \dfrac{(1 + R^2 e^{-(\alpha_L + \alpha_R)z_p} + TRe^{-\alpha_L z_p})(1 - e^{-(\alpha_L + \alpha_R)z_p})}{\alpha_L + \alpha_R} + \dfrac{R(e^{-2\alpha_L z_p} - e^{-2\alpha_R z_p}) + T(e^{-\alpha_L z_p} - e^{-\alpha_R z_p})}{\alpha_R - \alpha_L}$

TABLE II. Optimum fiber lengths.

Scattering geometry	Optimum physical fiber length	Maximum effective fiber length
Forward scattering $\alpha_L = \alpha_R$	$z_p = \dfrac{1}{\alpha}$	$z_e = \dfrac{0.368}{\alpha}$
Forward scattering $\alpha_L \neq \alpha_R$	$z_p = \dfrac{1}{\alpha_R - \alpha_L}\ln\left(\dfrac{\alpha_R}{\alpha_L}\right)$	$z_e = \dfrac{\left\{\left(\dfrac{\alpha_R}{\alpha_L}\right)^{-\alpha_L/(\alpha_R - \alpha_L)} - \left(\dfrac{\alpha_R}{\alpha_L}\right)^{-\alpha_R/(\alpha_R - \alpha_L)}\right\}}{\alpha_R - \alpha_L}$
Backward scattering $\alpha_L = \alpha_R$	$z_p \to \infty$	$z_e \to \dfrac{0.5}{\alpha}$
Backward scattering $\alpha_L \neq \alpha_R$	$z_p \to \infty$	$z_e = \dfrac{1}{\alpha_L + \alpha_R}$
Forward scattering with long-pass filter $\alpha_L = \alpha_R$	$z_p = \dfrac{0.802}{\alpha}$	$z_e = \dfrac{0.539}{\alpha}$
Backward scattering with distal end mirror $\alpha_L = \alpha_R$	$z_p = \dfrac{0.639}{\alpha}$	$z_e = \dfrac{0.817}{\alpha}$
Combined forward and backward scattering $\alpha_L = \alpha_R$	$z_p = \dfrac{1.278}{\alpha}$	$z_e = \dfrac{0.818}{\alpha}$

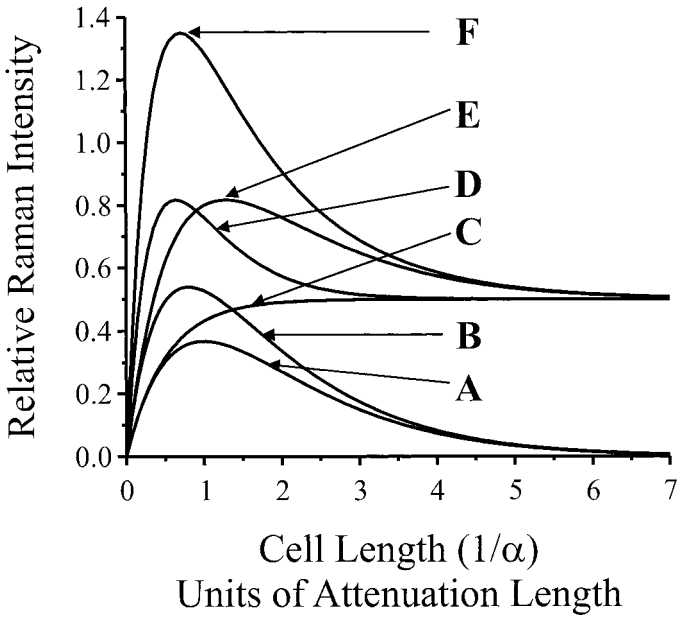

FIG. 3. Relative total Raman intensity emitted from LCOF sample cell vs. cell length. Here, the functional forms of z_e listed in Table I are plotted vs. z_p for each of the six scattering geometries. (***A***) Forward scattering; (***B***) forward scattering with long-pass filter; (***C***) backward scattering; (***D***) backward scattering with distal end mirror; (***E***) combined forward and backward scattering; (***F***) combined forward and backward scattering with long-pass filter.

system based only on knowledge of the intrinsic properties of the fiber, specifically the loss or attenuation coefficient, α, and inner diameter, *d*. Table II shows that the maximum z_e, and therefore maximum Raman intensity, regardless of scattering geometry, is inversely proportional to the loss coefficient, α. Thus, one may assume that the loss coefficient alone may be an appropriate figure of merit; however, this is not the case. It will be shown below that in many instances much, or most, of the Raman light emitted from an LCOF is lost in the process of coupling the light to the spectroscopic instrument. In developing a figure of merit, one must consider not only the total Raman intensity emitted from the cell but also the ''utilizable Raman intensity'', or the Raman intensity that can be coupled from the LCOF into the spectroscopic instrument in a particular optical arrangement. As stated explicitly in Eq. 10, the figure of merit should be directly proportional to the utilizable Raman intensity

$$\text{Figure of Merit} \propto \text{Utilizable Raman Intensity} = I_R \eta \quad (10)$$

where I_R is the total Raman intensity emitted from the LCOF and η is the coupling efficiency into the spectrometer or spectrograph. Here, we attempt to determine the figure of merit for an LCOF in a spectroscopic system based on a conventional double monochromator equipped with a photomultiplier tube detector. For simplicity, we consider only those geometries in which light is collected from a single end of the LCOF (Fig. 3A–3D).

Figure 4 displays a simplified schematic diagram of the conventional Raman system. For simplicity, only a single monochromator is shown, although a double monochromator was used in all the experiments presented here. In this system, the LCOF sample cell was operated in the forward scattering geometry shown in Fig. 2A. Figure 4 also defines a few of the optical parameters of the Raman system. The lens in front of the entrance slit was used to *f*/# match the LCOF to the spectrometer and consequently optimize the light collection. Through the process of *f*/# matching the LCOF to the monochro-

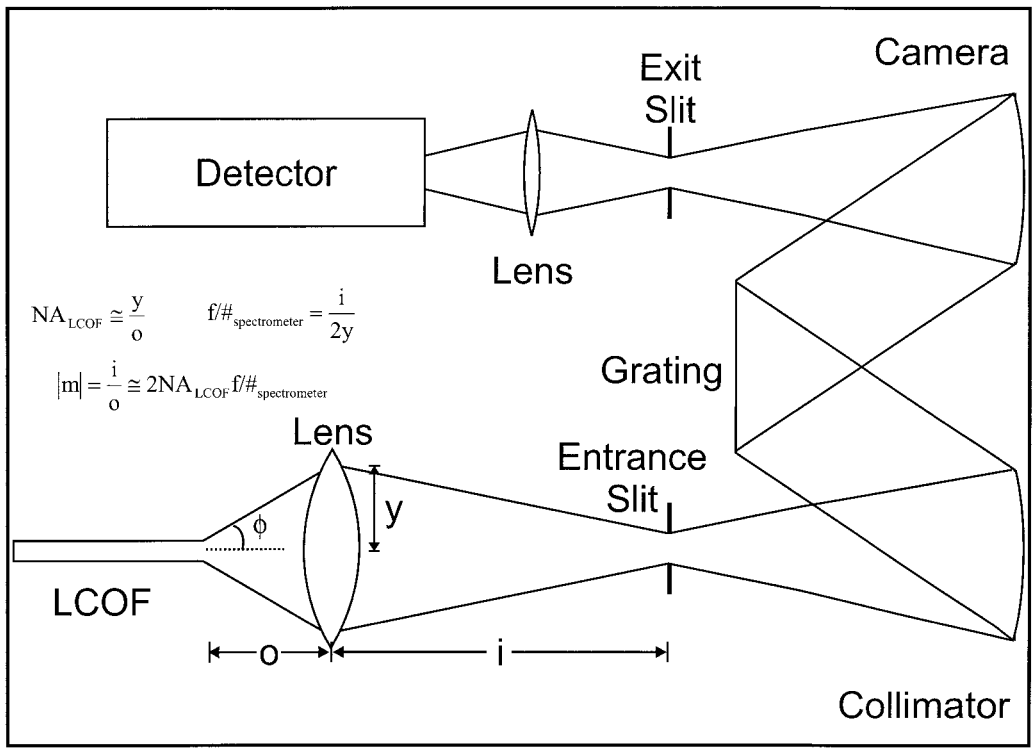

FIG. 4. Instrumental diagram of an LCOF Raman apparatus that uses a conventional monochromator optical system.

mator, the magnification of the emitted light at the spectrometer entrance slit can be calculated when the numerical aperture, NA, of the LCOF and the $f/\#$ of the spectrometer are known. The NA of the LCOF is defined by

$$NA_{LCOF} = n_{co}\sin\theta \quad (11)$$

where n_{co} is the refractive index of the core liquid and θ is the angle the light makes in the fiber with respect to the cladding, as is shown in Fig. 1. Using Snell's law,

$$n_1\sin\theta_1 = n_2\sin\theta_2 \quad (12)$$

one can calculate the value of the θ_2, the angle at which the light travels in the air as it exits the LCOF. In Figs. 1 and 4, θ_2 is labeled as ϕ. Assuming that $n_{air} = 1$, the combination of Eqs. 11 and 12 results in following expression:

$$NA_{LCOF} = \sin\phi \quad (13)$$

Snell's law can also be used to equate the NA_{LCOF} to

$$NA_{LCOF} = \sqrt{(n_{co}^2 - n_{cl}^2)} \quad (14)$$

For Teflon®-AF tubing filled with methanol or water, $NA_{LCOF} \cong 0.33$. Thus, ϕ is approximately 19°. At this value, $\sin\phi \cong \tan\phi$, which results in $NA_{LCOF} \cong \tan\phi \cong (y/o)$ where y and o are distances defined in Fig. 4. The $f/\#$ of the spectrometer is equal to the ratio of the focal length to the diameter of the mirror. From Fig. 4, this quantity is $(i/2y)$. Likewise, the magnification factor, m, of the source image at the entrance slits is defined by (i/o). Given that the $f/\#$ of the spectrometer $= (i/2y)$ and the $NA_{LCOF} \cong (y/o)$, the magnification can be expressed by the following equation:

$$|m| \cong 2NA_{LCOF} f/\#_{spectrometer} \quad (15)$$

Thus, for the double monochromator used here with $f/\# = 8$, the LCOF source was magnified by a factor of ~ 5.3. Therefore, even in the case of the smallest LCOF previously manufactured for this project ($d = 50$ μm), the magnified image of the source at the entrance slit was much larger than the slit width. When the image diameter is much larger than the slit width, the fraction of light entering the monochromator, or coupling efficiency, is given by

$$\eta = \frac{4w}{\pi D} = \frac{4w}{\pi|m|d} \quad (16)$$

where w is the slit width and D is the diameter of the source image at the slit, $D = md$. Figure 5 illustrates that η is the ratio of the slit area to the area of the magnified image. By combining Eqs. 10 and 16 with the maximum Raman intensity derived from the maximum z_e values listed in Table II, we see that the figure of merit for and LCOF in a single-ended collection geometry (Fig. 3A–3D) coupled to a conventional Raman spectrometer is given by

$$\text{Figure of Merit} = \frac{1}{\alpha d} \quad (17)$$

It should be emphasized that functional form of the figure of merit is specific to the excitation/collection/spectrometer geometry presented here (conventional spectrometer, direct imaging onto slit, slit length greater than diameter of LCOF image, etc.) In other systems—in particular, fiber optically coupled Raman systems—the form of the figure of merit will in general be different.[10]

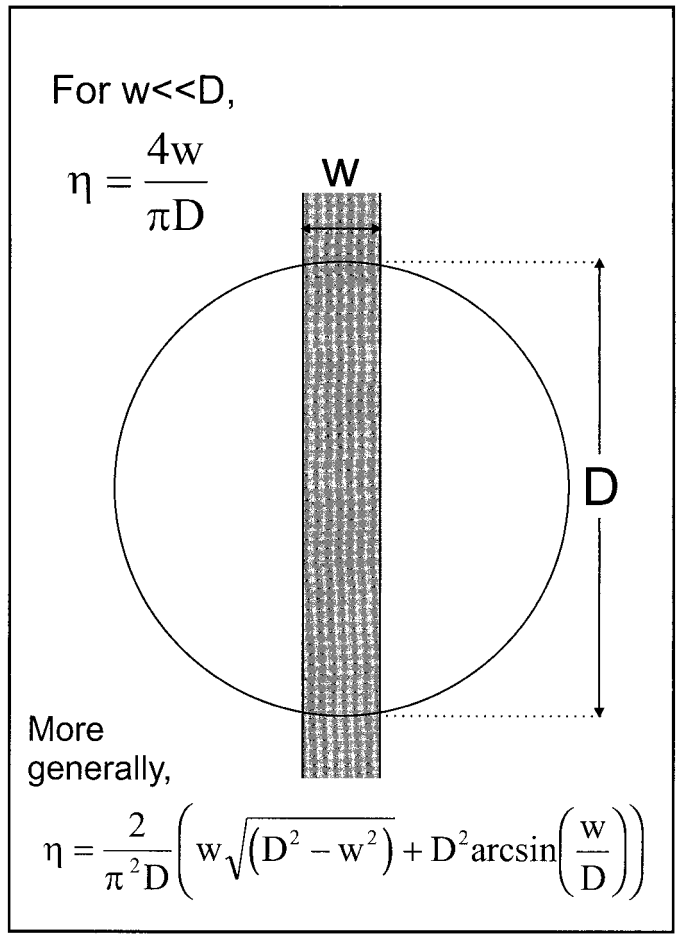

FIG. 5. Coupling efficiency, η, of the Raman light into the spectrometer. (Fraction of the light transmitted through the slit.)

To test the validity of Eq. 17, we performed several experiments with LCOFs of different inner diameters and loss characteristics. The LCOF cells were operated in the forward scattering geometry and were arranged in front of the double monochromator, as shown in Fig. 4. Forward scattering geometry was chosen solely for its simplicity. The LCOFs were filled with methanol, and the intensity of the 2834 cm^{-1} C–H stretching peak was measured as a function of cell length by using the 514.5 nm line of an argon-ion laser. The cell length was varied by adjusting the position of the glass optical fiber used to deliver the laser radiation inside the LCOF. The results of the intensity were plotted as a function of physical length and then fitted to the functional form given in Table I. The loss coefficient and maximum intensity were extracted from the fitting parameters. This process was done for LCOFs with different values of d and α. An example of the results from a single set of measurements is shown in Fig. 6. In order to obtain an appropriate range of data, several sections of tubing with a relatively large inner diameter were fabricated specifically for these experiments, and pieces of poor-quality tubing were chosen for their high loss. In many cases, especially for those involving poor-quality tubing, the data showed consid-

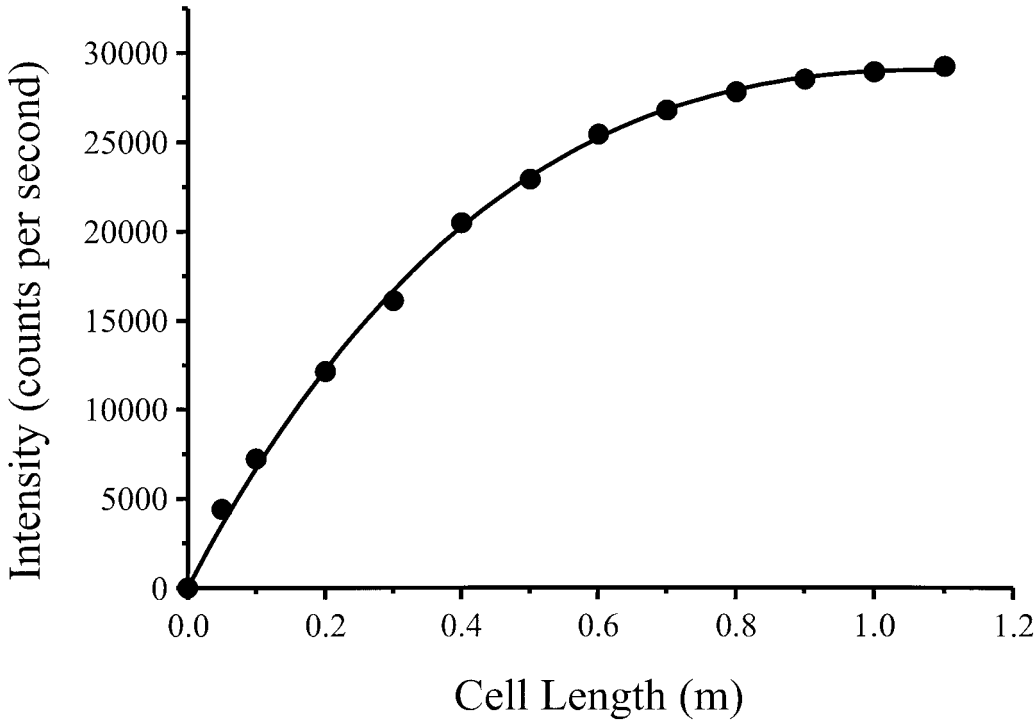

FIG. 6. Raman intensity (2834 cm^{-1} band) vs. physical cell length for 533 μm i.d. LCOF with methanol. Circles represent actual data points. The line is the best fit to expected functional form for forward scattering: $y = z_p e^{-\alpha z_p}$, where $\alpha = 0.933\ m^{-1}$.

erably more noise (see Fig. 7) than what is displayed in Fig. 6. The results of eight sets of experiments are summarized in Fig. 7, which plots the maximum normalized Raman intensity vs. the figure of merit ($1/\alpha d$). Normalization of the Raman intensity was achieved by dividing the Raman intensity at optimum cell length by the input laser power.

From Fig. 7, it appears that there is an approximately

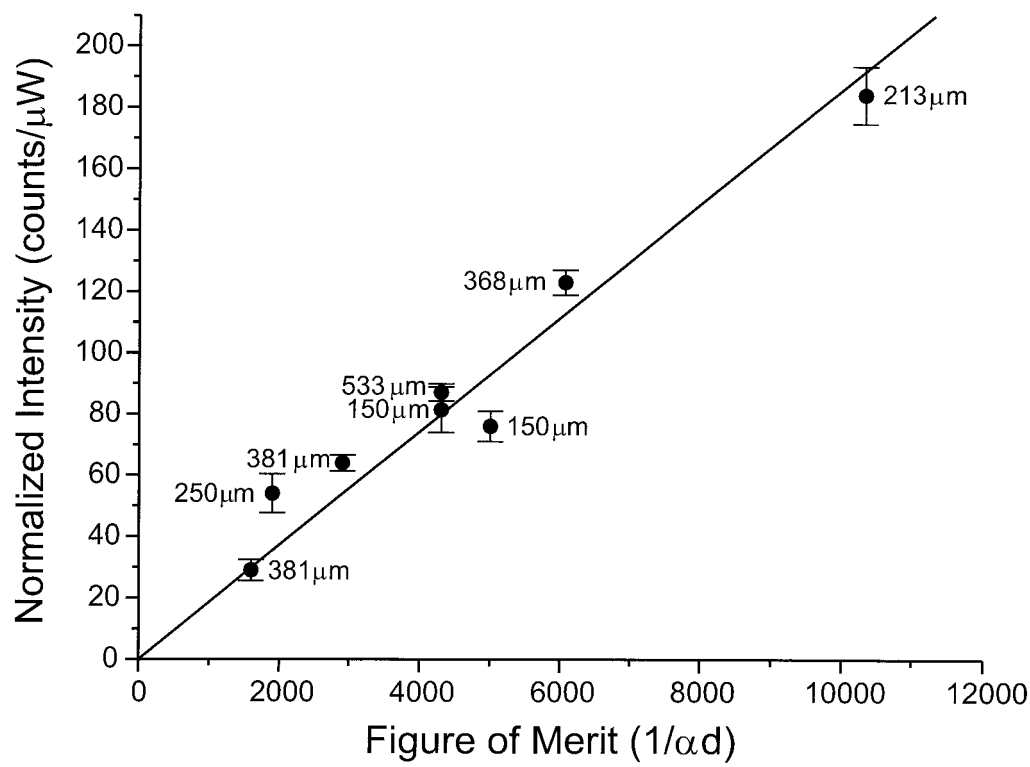

FIG. 7. Maximum normalized Raman intensity of the 2834 cm^{-1} band (counts per second per μW of laser power) vs. figure of merit for LCOFs filled with methanol. All Raman measurements presented here were collected by using 514.5 nm excitation and a conventional spectrometer. Data point labels indicate LCOF i.d.

linear relationship between the Raman intensity and the figure of merit. Thus, we believe that the expression given in Eq. 17 is correct for the conventional system used here. Scatter in the data can be attributed to noise in the Raman intensity vs. cell length data observed with poor-quality tubing, which led to larger error in determination of α. Given that the optical characteristics of Teflon®-AF LCOFs tend to vary significantly with parameters such as inside diameter, core liquid, excitation/emission wavelengths, and manufacturing technique, we believe that a figure of merit such as that derived here is essential for optimizing the performance of an LCOF accessory with a Raman system.

CONCLUSION

We have developed a method of estimating and optimizing the Raman intensity delivered by a Teflon®-AF LCOF to a spectroscopic instrument. By assuming that the intensities of both the laser and Raman scattered light undergo single exponential decay as they propagate through the waveguide, we derived expressions for an ''effective'' fiber length, z_e, for six commonly used scattering geometries. We showed that Raman intensity is directly proportional to this effective fiber length and is a function of the following paramters: (1) the loss coefficient of the LCOF at the laser and Raman wavelengths, (2) the physical length of the LCOF, (3) the sampling geometry, and (4) the input laser power. Raman intensities as a function of LCOF cell length were compared for six simple scattering geometries. For the general purpose of maximizing signal intensity, we conclude that a combined foward and backward scattering configuration that uses a long-pass filter is the theoretically ideal arrangement. At short LCOF lengths, this geometry can provide almost 40% more Raman intensity than other configurations. The second part of this report addressed the fraction of the Raman light emitted from the LCOF that can be coupled into a spectrometer. We developed a ''figure of merit'' which allows the designer/user of an LCOF Raman instrument to predict the relative performance of different LCOFs in a particular spectroscopic system. The figure of merit is simply the product of the total Raman light emitted from the LCOF and the coupling efficiency into the spectrometer. For the conventional double monochromator and $f/\#$ matching optics used here, we found that the LCOF source image at the spectrometer entrance slit was much larger than the slit width. Hence, only a fraction of the total emitted Raman light can couple into the spectrometer. Under these circumstances we found the figure of merit for an LCOF in a single-ended collection geometry to be simply $1/\alpha d$, where α is the loss coefficient and d the inside diameter of the LCOF.

Raman spectra of methanol were collected from eight different LCOFs of various inner diameters and loss coeffficients. A relatively linear relationship was observed when the normalized Raman intensities of the 2834 cm^{-1} peak were plotted vs. $(1/\alpha d)$. Hence, we conclude that our proposed figure of merit was indeed correct.

ACKNOWLEDGMENT

This work was supported by the National Science Foundation under Grant No. DMI-9705611.

1. P. Grassmann, Zeitschrift für Physik **72,** 240 (1931).
2. H. H. Cary, U. S. Patent 2,940,355 (1960).
3. R. C. Hawes, U. S. Patent 3,556,659 (1971).
4. J. Loader, *Basic Laser Raman Spectroscopy* (Heyden and Sons, London, 1970).
5. T. R. Gilson and P. J. Hendra, *Laser Raman Spectroscopy* (Wiley, London, 1970).
6. G. E. Walrafen and J. Stone, Appl. Spectrosc. **26,** 585 (1972).
7. J. Stone and G. E. Walrafen, U. S. Patent 3,770,350 (1973).
8. G. E. Walrafen, Phys. B1. **12,** 540 (1974).
9. R. I. Altkorn, I. Koev, R. P. Van Duyne, and M. Litorja, Appl. Opt. **36,** 8992 (1997).
10. R. Altkorn, I. Koev, and M. J. Pelletier, Appl. Spectrosc. **53,** 1169 (1999).
11. M. J. Pelletier and R. Altkorn, Appl. Spectrosc. **54,** 1837 (2000).
12. M. Holtz, P. K. Dasgupta, and G. Zhang, Anal. Chem. **71,** 2934 (1999).
13. L. Song, S. Liu, V. Zhelyaskov, and M. A. El-Sayed, Appl. Spectrosc. **52,** 1364 (1998).
14. R. J. Dijkstra, A. N. Bader, G. P. Hoornweg, U. A. T. Brinkman, and C. Gooijer, Anal. Chem. **71,** 4575 (1999).
15. B. J. Marquardt, P. G. Vahey, R. E. Synovec, and L. W. Burgess, Anal. Chem. **71,** 4808 (1999).
16. B. J. Marquardt, K. P. Turney, and L. W. Burgess, Proc. SPIE-Int. Soc. Opt. Eng. **3860,** 239 (1999).
17. J. U. White, N. L. Alpert, and A. G. DeBell, J. Opt. Soc. Am. **45,** 154 (1955).
18. G. E. Walrafen, Appl. Spectrosc. **29,** 179 (1975).
19. G. E. Walrafen, Appl. Spectrosc. **31,** 295 (1977).
20. G. E. Walrafen, U. S. Patent 4,012,147 (1977).
21. R. Altkorn, I. Koev, and A. Gottlieb Appl. Spectrosc. **51,** 1554 (1997).
22. IUPAC, Pure Appl. Chem. **67,** 1725 (1995).
23. B. Schrader, ''Tools for Infrared and Raman Spectroscopy'', in *Infrared and Raman Spectroscopy: Methods and Applications*, B. Schrader, Ed. (VCH, Weinheim, 1995), pp. 63–162.
24. H. W. Schrötter and H. W. Klöckner, ''Raman Scattering Cross Sections in Gases and Liquids'', in *Raman Spectroscopy of Gases and Liquids*, S. Brodersen, J. M. Friedman, H. W. Klöckner, G. V. Knighten, J. W. Nibler, D. L. Rousseau, H. W. Schrötter, R. P. Srivastava, A. Weber, P. F. Williams, and H. R. Zaidi, Eds. (Springer-Verlag, New York, 1979), pp. 123–166.
25. G. Eckhardt and W. G. Wagner, J. Mol. Spectrosc. **19,** 407 (1966).
26. J. R. Nestor and E. R. Lippincott, J. Raman Spectrosc. **1,** 305 (1973).
27. C. I. Carr, Jr., and B. H. Zinn, J. Chem. Phys. **18,** 1616 (1950).
28. A. W. Snyder and J. D. Love, *Optical Waveguide Theory* (Chapman and Hall, New York, 1983), p. 27.
29. S. V. Golovkin, A. M. Gorin, A. V. Kulichenko, A. E. Kushnirenko, A. I. Peresypkin, A. I. Pyshchev, V. I. Rykalin, and A. A. Zaichenko, Nucl. Instr. Meth. Phys. Res. A **305,** 385 (1991).
30. G. Barbiellini, A. Martinis, R. Sangoi, and F. Scuri, Nucl. Instr. Meth. Phys. Res. B **72,** 481 (1992).
31. W. P. Siegmund, P. Nass, J. P. Fabre, W. Flegel, V. Zacek, G. Martellotti, and G. Wilquet, Proc. SPIE-Int. Soc. Opt. Eng. **1737,** 2 (1992).